Geophys. J. Int. (2000) **141,** 241–252

Analysis of seismological and geological observations for moderate-size earthquakes: the Colfiorito Fault System (Central Apennines, Italy)

Salvatore Barba and Roberto Basili

Istituto Nazionale di Geofisica, Via di Vigna Murata, 605, 00143 *Roma, Italy. E-mail: barba@ingrm.it; basili_r@ingrm.it*

Accepted 1999 November 18. Received 1999 September 30; in original form 1998 December 15

SUMMARY

To contribute to the understanding of the relationships between moderate earthquakes and the faults that are recognizable in the geological record, we analysed seismological and geological data related to the 1997–1998 Umbria-Marche (Central Italy) earthquake swarm. The seismological recordings, collected by local networks, allowed accurate location of about 1000 events, whereas the geological field observations provided a picture of the structural features and the ground-surface deformations. We also re-examined and used some published data and results, mostly about the fault plane solutions and the geology.

On the basis of earthquake locations, fault plane solutions, and geological mapping we explored the possible correlation between the earthquake causative fault planes and the normal faults exposed in the area. Our results show that the two main shocks that occurred on 1997 September 26 ($M_W = 5.7$ and $M_W = 6.0$) originated on the same structure, reactivating at depth the Colfiorito normal faults. Neither rupture propagated up to the ground surface, but both triggered gravitational sliding that occurred along pre-existing fault scarps. The earthquake that occurred on 1997 October 14 ($M_W = 5.6$) originated on another fault branch at a much shallower depth. In spite of its lower magnitude, this earthquake produced tectonic ruptures where the fault plane projects to the surface in an area where no faults were previously mapped.

By comparing the palaeostress reconstruction, based on slickenside lineation analysis, and the focal mechanism solutions, we suggest a possible correlation between the long-term (Early Middle Pleistocene) cumulative effects of the Colfiorito Fault System and the short-term behaviour of the fault planes observed during this earthquake swarm, favouring the idea of a seismogenic source producing clustered moderate-size earthquakes rather than large events scattered in time.

Key words: Central Apennines, earthquake, Italy, normal faulting, seismotectonics.

INTRODUCTION

Empirical relationships between earthquake magnitude and rupture dimensions (Bonilla *et al.* 1984; Bonilla 1988; Wells & Coppersmith 1994) show that for magnitude $M < 6$ the signature at the ground surface of coseismic ruptures is very faint. Such ruptures fall in the size range of many other surface deformation features that could have their origin in ground shaking, and therefore it could be very difficult to detect them in the field and to identify correctly the active faults. In regions characterized by a moderate level of seismicity, the long-term cumulative effects of coseismic ruptures could give rise to unclear structural patterns, which, in turn, greatly hinder the understanding of the overall seismotectonic setting. Nevertheless, $M > 5$ multiple earthquakes are able to produce severe damage and therefore are of great societal interest.

The area where the 1997–1998 Colfiorito earthquakes occurred (Umbria-Marche region, in the northern part of the Central Apennines, Fig. 1) is a typical example of the problem described above. On one side, several moderate earthquakes struck this area in historical time (Boschi *et al.* 1997), while instrumentally detected sequences occurred in 1979 near

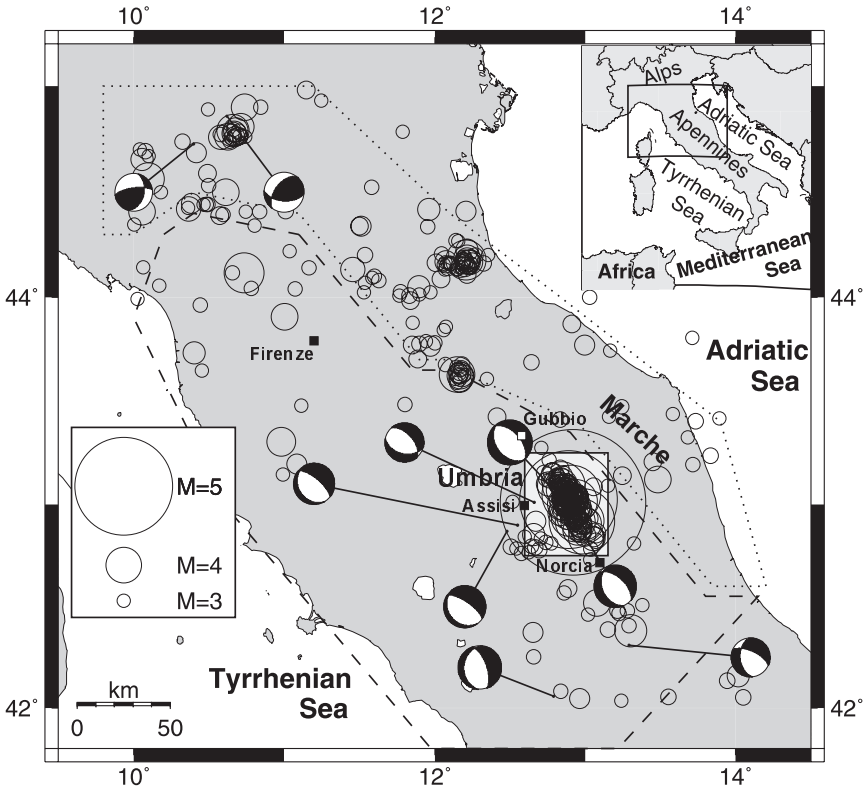

Figure 1. Sketch-map showing extensional (dashed line) and compressional zones (dotted line) within the northern Apennine chain. The light-grey rectangle (enlarged in subsequent figures) contains the earthquakes analysed in this paper. CMT solutions are after the Harvard catalogue (Dziewonski & Woodhouse 1983; http://www.seismology.harvard.edu/CMTsearch.html).

Norcia (main shock $M_S = 5.8$, Deschamps *et al* 1984), about 30 km southeast of Colfiorito, and in 1984 near Gubbio (mainshock $M_S = 5.3$, Haessler *et al.* 1988), about 45 km to the northwest. On the other side, many Quaternary normal faults characterize the tectonic setting of the region (from north to south: Menichetti 1992 for the Gubbio area; Bosi *et al.* 1983, unpublished map of the Gualdo Tadino zone; Calamita & Pizzi 1992 and Cello *et al.* 1997 for the southern zone). Such faults are generally up to 15 km long, strike NW–SE, plunge SW, and have mainly dip-slip kinematics. Cello *et al.* (1997) report also N–S-trending left-lateral strike-slip faults. GPS-based methods have not yet allowed extension loci to be isolated, probably because of the low extension rate and the mainly vertical tectonics. In fact, the relationship between outcropping and seismogenic faults is not yet clear.

The seismic swarm analysed in this work began on 1997 September 3, and during the subsequent two months it was characterized by more than 25 earthquakes with $M > 4.0$.

On 1997 September 26, two earthquakes occurred near the village of Colfiorito, the first at 00:33 GMT ($M_W = 5.7$) and the second at 09:40 GMT ($M_W = 6.0$), causing severe damage, a few casualties and many injuries. The socio-economic life of this historical district was literally shaken, and its major symbol, the Basilica of San Francesco in Assisi, was severely damaged. On October 14 at 15:23 GMT another $M_W = 5.6$ earthquake occurred about 15 km to the south, near the village of Sellano. During the following few months the seismic activity continued to the northwest, extending the fractured area by more than 50 km.

Starting just after the first main shock, several field surveys were carried out in the epicentral area by various research institutions, and seismological data were collected by temporary weak- and strong-motion networks managed by the Istituto Nazionale di Geofisica (ING) and Servizio Sismico Nazionale (SSN), deployed to improve permanent station coverage (Barba *et al.* 1995; Berardi *et al.* 1998). Geological investigations along with geodetic measurements were conducted by the Istituto Geografico Militare, Gruppo Nazionale per la Difesa dai Terremoti (GNDT), ING, and Agenzia Nazionale Protezione Ambiente in order to collect data concerning geological effects and surface deformation features. A macroseismic survey, mainly conducted by SSN, provided a detailed picture of damage distribution (see Camassi *et al.* 1997).

These surveys provided all the necessary data for a thorough description of the Colfiorito Fault System (CFFS) from different points of view. Most of the seismicity is dealt with in Amato *et al.* (1998) and Cattaneo *et al.* (1998a,b), while source properties and kinematics are analysed by Zollo *et al.* (1998, 1999), Pino *et al.* (1999), Ekström *et al.* (1998), and Olivieri & Ekström (1999). The analysis of geological features is treated in Basili *et al.* (1999), Cinti *et al.* (1999), Cello *et al.* (1998), and Meghraoui *et al.* (1998). The results of geodetic observations, such as SAR interferometry, GPS data analysis and topographic levelling, are discussed by Stramondo *et al.* (1999), Hunstad *et al.* (1998), Basili & Meghraoui (1999), and De Martini *et al.* (1999), refining the picture of coseismic surface deformations.

Despite the large number of studies, many of which are still in progress, the relationships among (1) the seismogenic faults and their behaviour, (2) the earthquake signatures at the surface, and (3) the correlative structures recorded over geological time are not yet clear. Because directivity of the source and distance from the fault greatly influence the probable ground motion, i.e. the seismic hazard, it is necessary that relationships among points (1)–(3) be better understood. To this end, we will try also to address the controversy among Basili *et al.* (1998), Cinti *et al.* (1999), and Cello *et al.* (1998).

This paper combines seismological and geological data in order to contribute to the understanding of the role played during the seismic swarm by the faults exposed in the area and belonging to the CFFS. To this end, we have both reinterpreted some published data and analysed new ones. Results suggest how and to what extent the integration of geological and seismological measurements constrains the seismotectonic interpretations and provides a reliable basis for the assessment of seismic hazard.

GEOLOGICAL BACKGROUND

The northern Apennines are an east-verging fold-and-thrust mountain belt overriding and accreting on the subducting Adria plate. Compressional tectonics showed an eastward migration, all through the Tertiary (66–1.81 Ma) and the Quaternary (< 1.81 Ma), affecting Mesozoic–Palaeogene (> 30 Ma) passive margin carbonate sequences and Chattian–Pleistocene (< 30 Ma) fore-deep terrigenous sequences. In addition to compression at the thrust leading edge, the mountain belt also experienced coeval back-arc extension combined with regional crustal uplift (Doglioni 1997).

The area affected by the 1997–1998 series of earthquakes is an elevated region at the rear of a long-wavelength anticline (Calamita & Pizzi 1992) located just to the west of the current transition between the extensional and compressional stress regimes (Fig. 1).

As recently shown by deep seismic reflection profiles (Pialli *et al.* 1991; Barchi *et al.* 1997), extension in this region was driven along low-angle (~20°–30°) east-dipping master normal faults. A number of antithetic (west-dipping) high-angle (~40°–60°) dip-slip normal faults join the masters within the top 10–15 km of the crust (Doglioni *et al.* 1997; Boncio *et al.* 1997), thereby forming a series of intermontane basins which alternate with NW–SE-trending ranges. These last steeper faults lay at the eastern boundaries between the intermontane basins (half-grabens) and the surrounding uplands and left a strong imprint on the geological and geomorphic record by controlling drainage and continental sedimentary in-fill.

There are two main continental basins, which are clearly controlled by the CFFS: the Cesi-Forcella basin to the south, and the Colfiorito basin to the north (Fig. 2). The southern basin probably developed in a dominant interior drainage system, which is now captured at the south end by headward erosion of a N–S-trending valley. Late erosion contributed to exposing an Early Middle Pleistocene sedimentary basin filling (Ficcarelli *et al.* 1997), which unconformably rests on the carbonate bedrock. The in-fill consists mainly of lacustrine clay sequences interbedded with fluvial pebble/gravel lenses. This sequence is capped by a palustrine deposit containing a 424-ka-old pyroclastic layer (Ficcarelli *et al.* 1997) and, locally,

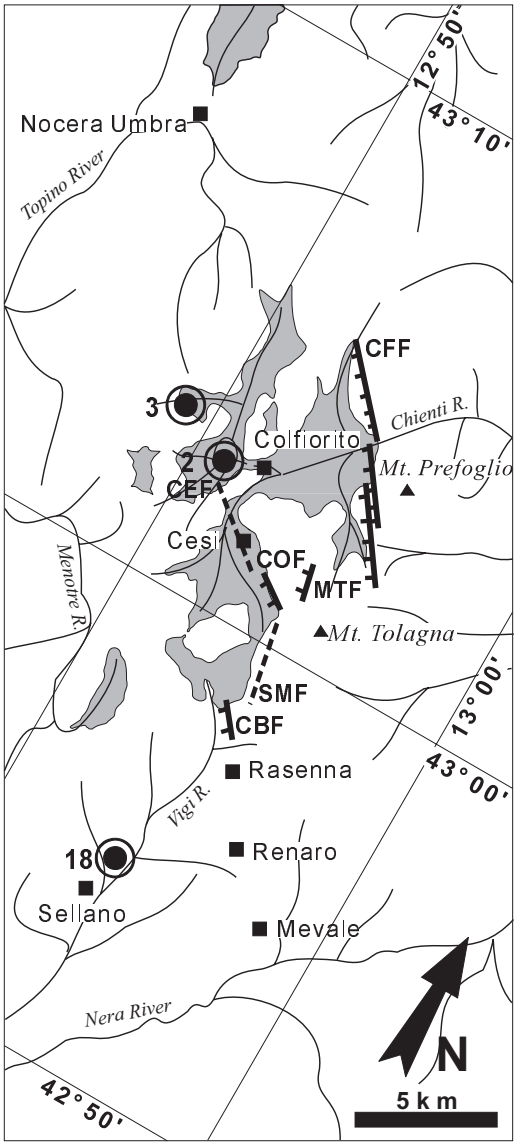

Figure 2. Sketch-map of the area struck by the Colfiorito earthquakes showing the CFFS, the drainage network, the main Quaternary basin deposits (grey), and the locations of main shocks listed in Table 1.

by Late Pleistocene alluvial fans. The Colfiorito basin, to the north, also developed in a dominant interior drainage system, but the sedimentary filling is much less exposed due to the absence of a deep-incising fluvial network. However, some Middle Pleistocene alluvial terrace deposits (Coltorti & Dramis 1988) are exposed in the peripheral area of the basin, while in the middle a few outcrops provide sightings of lacustrine clay sequences interbedded with fluvial gravel lenses. Lake environment persisted during the Holocene, and the basin was artificially drained in historical time.

STRUCTURAL ANALYSIS

The main exposed faults of the area are approximately 5–8 km long, strike between 120° and 170° north, plunge to the W–SW, and dip about 50°–60°. At the outcrop scale, the faults are marked by gouge several tens of metres thick, and by bedrock

fault scarps a few metres high. Taking into account the age of the sedimentary in-fill of the basins, and according to most of the geological literature of the region, these faults could be considered as representatives of the current stress regime, which has been active for approximately the last 800–1000 kyr (Early Middle Pleistocene). Recent activity of these faults is also indicated by faulted Late Pleistocene deposits (Cello *et al.* 1997).

Data concerning micro- and meso-scale structural features (Angelier 1984; Hancock 1985) were collected to analyse the distribution of slip along the fault traces and to reconstruct the palaeostress field of the area (Figs 2 and 3). The fault-slip data set comprises slickenside lineations measured at 12 sites along the main fault branches exposed in the area shown in Fig. 2, and at several minor outcrops. Slip data were collected on principal and auxiliary shear planes exposed on the face of bedrock fault scarps or embedded in the gouge. Although secondary structural features related to the activity of the CEF and SMF fault branches (dashed lines in Fig. 2) affect Quaternary deposits of the Cesi basin (mainly tilted clay deposits), the intervening fault surfaces are very poorly exposed and no data regarding these faults were collected.

Two subsets have been selected from the entire data set. The first includes the population of mesoscale faults measured at several sites along the CFF. The second includes those along the CBF. Only measurements of accurately determined slip have been taken into account, and slip observed at minor outcrops has been used only to verify the consistency of the entire data set. For these reasons, weights were kept equal to 1 in each data set in this analysis.

Reduced stress tensors were computed by direct inversion following the approach described by Angelier (1990) and using the program DAISY (Salvini 1998). The trend and plunge for σ_1, σ_2 and σ_3 (t_1, p_1; t_2, p_2; t_3, p_3) at CFF is (089, 82; 304, 06; 213, 04), at CBF it is (145, 65; 312, 24; 044, 05), and the total is (119, 84; 297, 06; 027, 00), with a ratio $\Phi = (\sigma_2 - \sigma_3)/(\sigma_1 - \sigma_3)$ of 0.303, 0.448, 0.266, respectively. Stereonet projection of fault slip data (Fig. 3) exhibits a good fit between the distribution of the observed slip and the computed shear stress. In addition, all three solutions exhibit a shape ratio Φ that assumes low values ($\Phi \sim 0.4$) and show similar attitudes of the tension axis, suggesting a good level of homogeneity in the data set and indicating that the solutions are stable. Coherence among the solutions of the two subsets and the total data set enables us to deduce that the examined fault branches belong to the same generation of faults, and therefore that the entire CFFS is controlled by a stress field that has a NE–SW-striking tension axis with a slight sinistral component.

SEISMOLOGICAL OBSERVATIONS

Teleseismic observations have shown that the slip and centroid of the three $M > 5.5$ events are shallower than the hypocentre depth (Olivieri & Ekström 1999), thus implying an upward

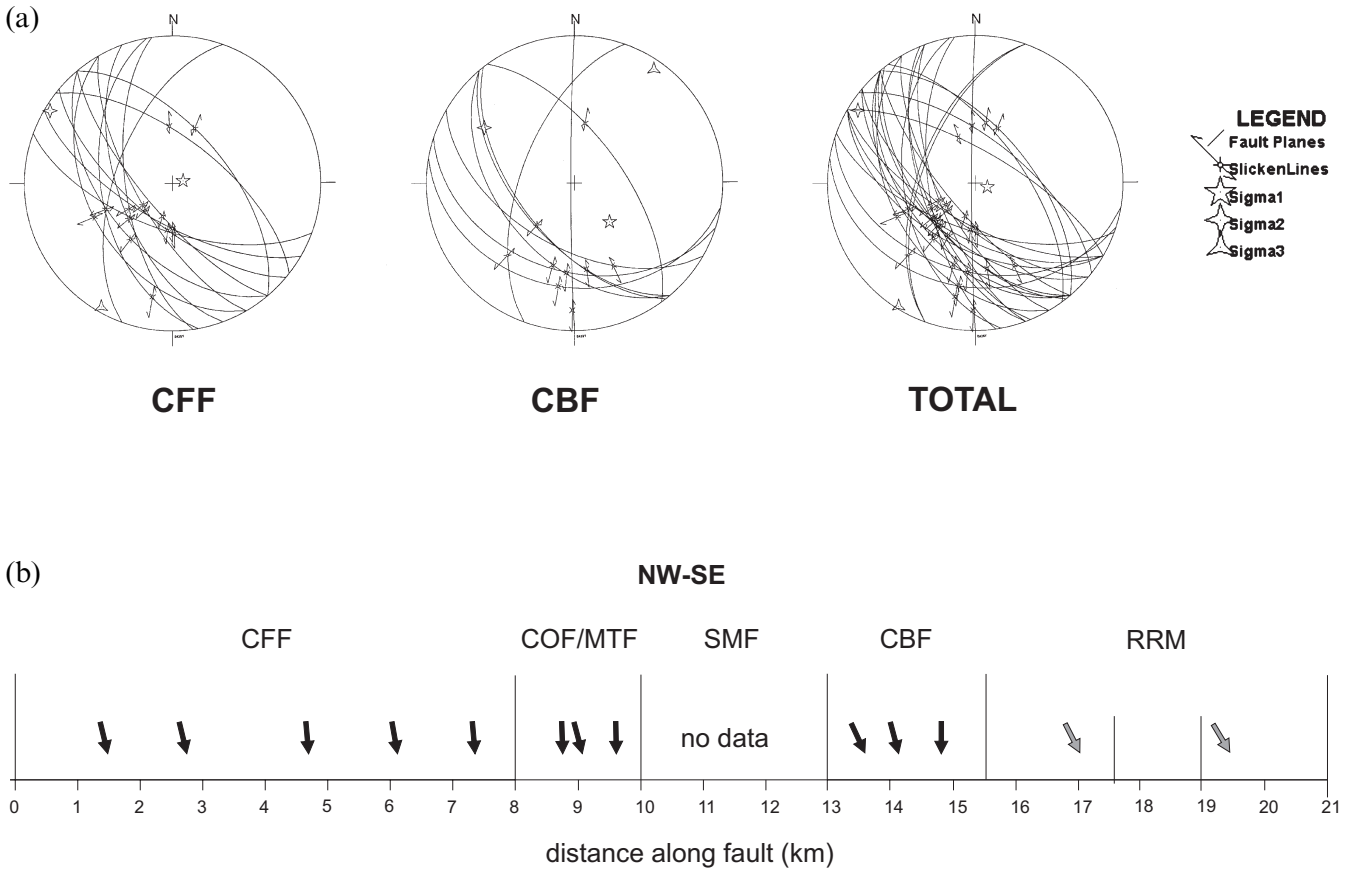

Figure 3. (a) Stereographic projections of fault slip data measured along the main fault branches exposed in the area shown in Fig. 2 and at several minor outcrops; principal stress axes are also shown. (b) Distribution of average slip data along-strike in the CFFS (black arrows), and slip of the RRM surface ruptures (grey arrows).

directivity of the sources. Because the slip is confined to the shallower portion of the crust, it is important to understand the possible relations between these earthquakes and their geological signature. To this end, we analysed details of fault geometry and kinematics of the three $M > 5.5$ events (see Table 2 for a summary) and located about 1000 $M > 2$ events, shown in Fig. 4, among which 26 were $M \geq 4$ (see Table 1).

Three SSN local seismic networks operating in the Umbria, Marche and Abruzzi regions, composed of 40 three-component short-period seismometers, and the ING network (Fig. 4) provided digital recordings from 1997 September 3 onwards. Up to 66 phase readings per event were accurately picked in a 110 km radius circle around Colfiorito. This data set allowed $M > 2$ events to be located with adequate accuracy on the horizontal plane (see next paragraph for a discussion of errors).

To compare the main ruptures with the exposed faults, it is important to assess the depth distribution of such events. The favourable experimental framework and the availability of a velocity model (hereinafter P90) derived from deep seismic refraction studies in the area (Ponziani *et al.* 1990) permitted a reasonable estimate of hypocentral depths of most events.

In order to apply such a detailed model (see Fig. 5) to generic hypocentre location, the number of layers found in P90 was reduced, combining two or more layers into one and assigning an average velocity to the resulting layer; the new simpler model shows a more uniform ray-path density in each layer. As the hypocentral depth of the biggest events was about 8 km, the discontinuity that the model shows at that depth was avoided by introducing a new interface at 4 km. Artificial clustering of hypocentres at 8 km has thus been reduced.

In order to utilize P90 in a complex tectonic environment such as the CFFS, we have to take into account the 3-D effects of the velocity structure, mainly the result of a lateral lithological contrast (Filippi & Alessandrini 2000) and the presence of Quaternary loose deposits. A trial and error procedure was carried out to reduce RMS residuals by varying velocities and to evaluate static station corrections. In this way, the use of a 3-D velocity model is avoided thus preserving location stability. The initial and the final models are shown in Fig. 5. We remark that we did not try to determine any new velocity model for the area, and that the procedure applied here only allowed the existing velocity model to be appropriate for hypocentre locations. Although a joint hypocentral determination technique would highlight tectonic alignments, we did not attempt it, because it was not needed for the purpose of this paper.

All events have been located using the HYPOCENTER program (Lienert *et al.* 1988). Phase weights have been established according to the reading uncertainty and to the hypocentral

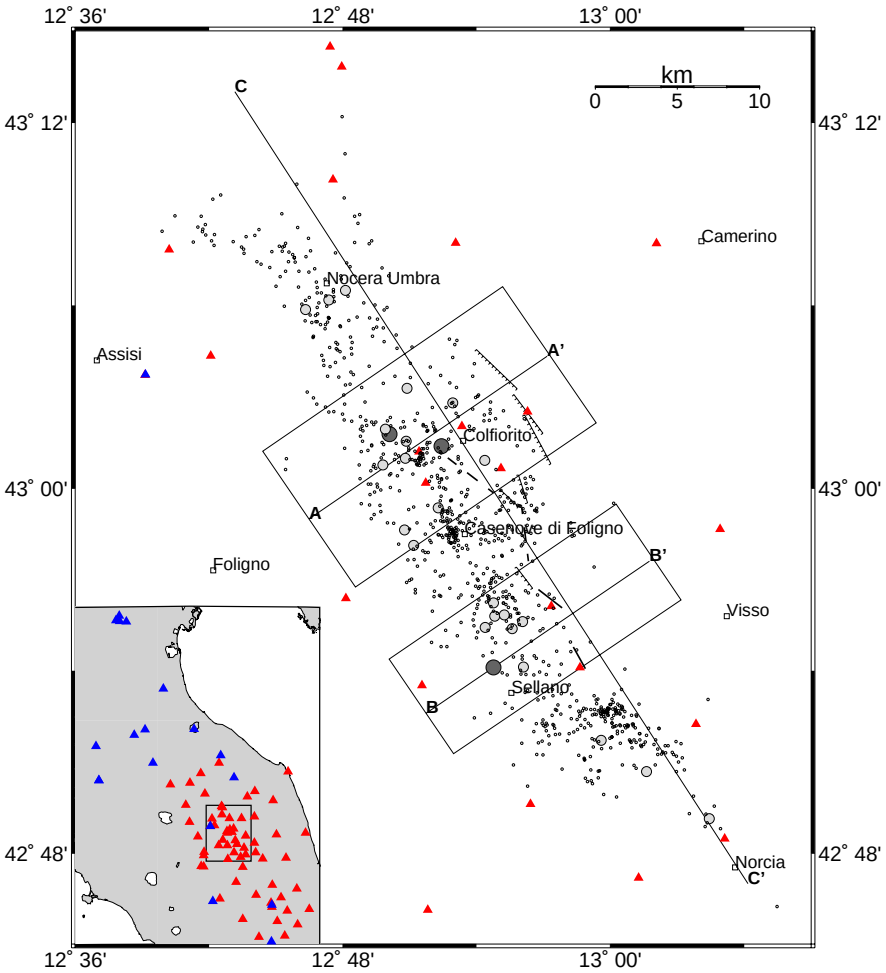

Figure 4. Map view of the 1997 Colfiorito swarm. Dark-grey circles: $M > 5.5$; light-grey circles: $M \geq 4$ (recorded between 1997 September 3 and 1997 December 31); small white circles: $M > 2$ (recorded between 1997 September 28 and 1997 December 31). Triangles represent SSN and ING seismometers that provided at least one phase reading.

Table 1. List of $M \geq 4$ earthquake solutions. Magnitudes M_L, M_W and M_D are labelled, respectively, with L, W, D (M_L and M_D from ING, M_W from Ekström *et al.* 1998). The magnitude of event number 4 cannot be determined from our records, because of the coda of earthquake number 3. A rough estimate of that magnitude indicates a value of $M \approx 5$, taking into account the damage caused by that earthquake and reported by P. Galli (personal communication). Gap: maximum azimuthal gap between stations in degrees; Rms: RMS residual of the location; Erh and Erz: errors on the horizontal and vertical planes, respectively.

Event No.	Date	Origin time (GMT)	Lat	Long	Depth (km)	Mag	No. obs.	Gap	Rms (s)	Erh (km)	Erz (km)
1	970903	22:07:29.83	43°00.99	12°50.80	9.1	4.5 W	37	158	0.23	0.9	0.6
2	970926	00:33:12.89	43°01.38	12°52.42	7.0	5.7 W	58	42	0.30	0.7	0.9
3	970926	09:40:26.73	43°01.78	12°50.09	8.0	6.0 W	42	33	0.32	1.0	1.1
4	970926	09:47:38.29	43°06.18	12°47.38	7.2	Unk	22	199	0.23	1.5	1.7
5	970926	13:30:52.45	43°00.92	12°54.37	6.1	4.5 W	30	125	0.29	1.1	1.1
6	970927	08:08:07.93	43°06.50	12°48.12	5.6	4.3 L	33	89	0.22	0.6	0.9
7	970927	19:56:43.38	43°03.29	12°50.88	5.8	4.0 L	42	65	0.25	0.6	0.8
8	970928	11:24:31.91	42°58.64	12°50.77	4.0	4.0 L	36	105	0.28	0.9	1.0
9	971002	10:59:56.27	43°05.86	12°46.34	6.5	4.1 L	72	36	0.27	0.5	0.5
10	971003	08:55:22.02	43°01.95	12°49.90	5.7	5.2 W	68	43	0.28	0.5	0.7
11	971004	06:49:59.49	42°55.43	12°54.39	5.9	4.1 D	66	88	0.22	0.5	0.6
12	971004	15:07:21.01	42°55.80	12°54.81	6.1	4.2 L	73	57	0.27	0.5	0.6
13	971004	16:13:32.97	42°55.84	12°55.25	3.5	4.7 W	71	56	0.34	0.7	0.7
14	971004	18:47:47.87	42°55.62	12°56.06	3.5	4.1 L	64	57	0.23	0.5	0.8
15	971006	23:24:53.23	43°00.76	12°49.79	7.4	5.4 W	70	46	0.24	0.5	0.5
16	971007	05:09:57.03	43°01.54	12°50.84	6.4	4.5 W	71	68	0.22	0.5	0.6
17	971012	11:08:36.87	42°54.13	12°56.10	2.6	5.2 W	60	61	0.35	0.7	0.7
18	971014	15:23:10.61	42°54.11	12°54.75	5.5	5.6 W	66	61	0.29	0.8	1.0
19	971015	22:53:10.78	42°55.39	12°55.59	5.6	4.1 L	64	86	0.24	0.5	0.6
20	971016	04:52:55.66	42°56.23	12°54.75	2.1	4.3 W	61	80	0.20	0.4	0.4
21	971016	12:00:31.54	43°02.81	12°52.92	5.6	4.5 L	71	46	0.46	0.8	1.1
22	971019	16:00:17.59	42°58.13	12°51.18	6.9	4.2 W	92	46	0.23	0.4	0.4
23	971020	01:27:04.93	42°59.35	12°52.27	6.1	3.8 D	94	44	0.22	0.4	0.5
24	971025	03:08:06.15	42°49.14	13°04.43	2.2	3.9 D	90	25	0.28	0.4	0.4
25	971109	19:07:33.67	42°51.71	12°59.59	3.0	4.6 D	59	93	0.43	0.8	0.8
26	971231	16:02:15.60	42°50.69	13°01.61	7.7	4.0 D	31	94	0.46	1.4	1.7

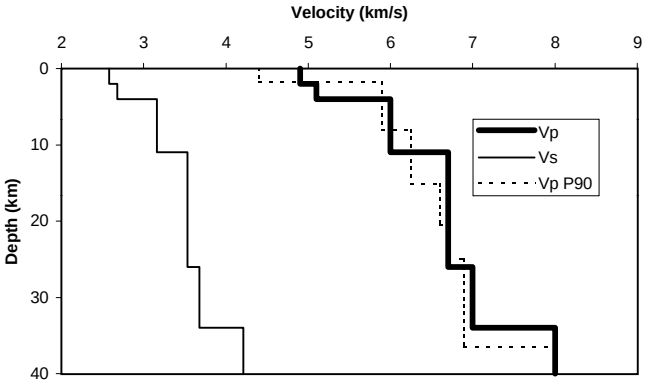

Figure 5. Velocity model used to locate all events analysed here. P90 refers to the model derived by Ponziani *et al.* (1990). $V_P/V_S = 1.9$ is assumed to be constant.

distance (weights have been assumed to be equal to 1 up to 40 km from the hypocentre, and then to decrease linearly, down to 0, with increasing distance up to 100 km). Outliers showing residuals greater than 1 s have been weighted out. The velocity model, the weighting criteria and the outlier removal threshold have been established on the basis of accurate analysis of the $M \geq 4$ events (listed in Table 1), and then applied to the $M < 4$ ones.

Initial solutions in the iterative location procedure have been chosen according to the 'S-P solution' on the horizontal plane and in accordance with the behaviour of the RMS residual versus depth. Location errors have been computed using the standard procedure of HYPOCENTER (Lienert *et al.* 1988) and then verified for the $M > 5.5$ events, following the approach discussed by Di Giovambattista & Barba (1997).

Source kinematic properties (Zollo *et al.* 1998, 1999) for the three $M > 5.5$ events are listed in Table 2 and represented in Fig. 6. Depths of major events (numbers 2, 3 and 18) are compatible with those estimated by strong-motion accelerometer data (Zollo *et al.* 1999) in the limit of measurement errors. Earthquake locations are shown in vertical sections in Figs 7 and 8.

Table 2. Summary of source properties of $M_W > 5.5$ events (numbers 2 and 3 taken from Zollo 1999, number 18 from Zollo *et al.* 1998 *L*: fault length along strike; *W*: width along dip; V_R: rupture velocity. Note that the bottom of the fault plane coincides with the focal depth.

Evt No.	Strike	Dip	L (km)	W (km)	V_R (km s^{-1})
2	148°	36°	6	6	3
3	152°	38°	12	7.5	2.6
18	144°	40°	6	6	

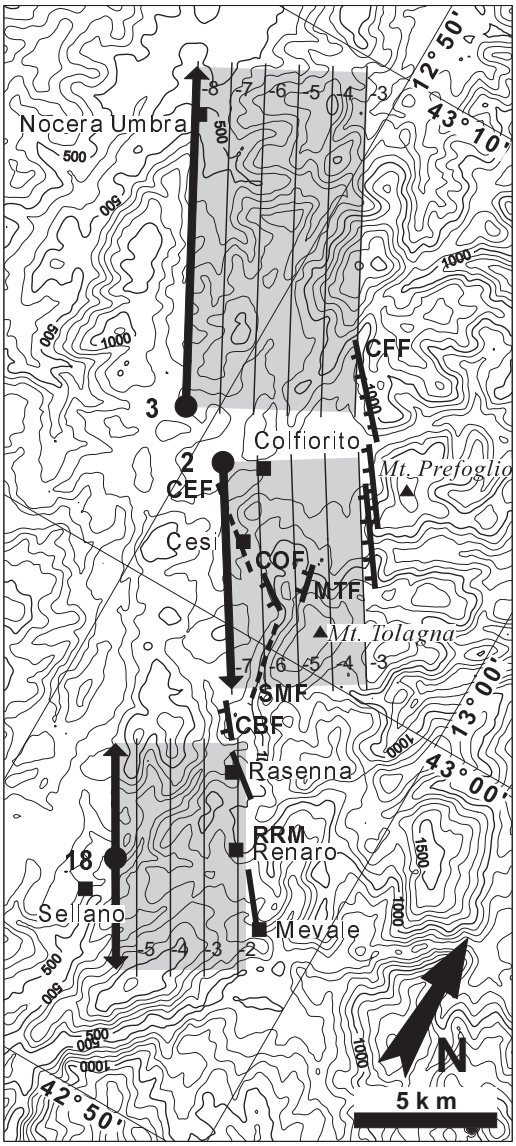

Figure 6. Map of the earthquake area. Contours are from a digital elevation model (grid 230 × 230 m). Fault plane solutions after Zollo *et al.* (1999) have been projected on the surface in dark grey with iso-depths. The arrows indicate source directivity, according to strong-motion data from SSN.

ON THE INFLUENCE OF MEASUREMENT ERRORS

Standard procedures of instrumental data inversion are usually affected by several sources of errors, which in turn affect interpretations. In this section, we will evaluate the influence of location errors, on the horizontal and vertical planes (Table 1), and of the uncertainties associated with the source parameters on our results.

We derived which faults could have been reactivated during the earthquake swarm from the epicentre distribution (Fig. 4), assuming that a SW-dipping normal fault can probably be considered active if it delineates the seismicity distribution. Since the spacing between the mapped normal faults is much greater than the earthquake location errors on the horizontal plane, interpretations based on earthquake locations will not change if the epicentres vary within the measurement errors.

In order to better constrain depths of $M > 5.5$ earthquakes, we evaluated the influence of different initial depths on final ones. The good geometry of the network (gaps lower than $\sim 60^\circ$ for $M > 5.5$) and the condition that the final solution was close to the one inferred by strong-motion analysis (Zollo *et al.* 1999) allowed errors of ± 1 km. To address the influence that errors associated with arrival times and with the velocity model have on depth, we used the method of Di Giovambattista & Barba (1997) and concluded that depth uncertainties are unvarying from NW to SE of Colfiorito. This observation supports conclusions based on the differences in the average depth from NW to SE. Smaller earthquakes ($M \leq 5.5$) have been considered to be affected by standard errors, and the depth of any specific $M \leq 5.5$ earthquake was never used to draw any conclusion. Only the average behaviour of low-magnitude seismicity with regard to its depth has been taken into account. As an example, the deepening of seismicity towards the SW (Fig. 7) or towards the NW (Fig. 8b) from the Colfiorito fault can be considered as 'average behaviour'.

To evaluate empirical errors on source properties we compared results drawn by completely different approaches. The kinematic model (Zollo *et al.* 1998, 1999) and the static model (Hunstad *et al.* 1998) show a difference of ± 2 km in fault width, which does not change conclusions on which fault plane ruptured. Moreover, both works state that the maximum slip is modelled to be in the first segment of fault number 3. The slip distribution along the fault inferred from the work of Zollo *et al.* (1999) is shown in Fig. 9.

The errors discussed in this section do not change the conclusions drawn from the results.

EARTHQUAKE GEOLOGICAL EFFECTS

In this section we adopt and review the descriptions of geological effects reported in Basili *et al.* (1998), which result from field surveys that were carried out just after the various earthquakes. We also summarize the criteria used to determine whether the faults broke the ground surface and to assess types and size of surface deformation.

Apart from the typically gravity-controlled deformations, such as landslides and associated features, that were scattered all over the surveyed area, two main types of surface brittle deformation were detected. The first type (A) consists of offsets between bedrock and slope deposits which occurred in the vicinity of possibly reactivated faults. This type of deformation was eventually interpreted as having been induced by ground shaking and clearly controlled by gravity. The second type (B) is that of tectonically originated ruptures, consisting of coseismic displacements of bedrock. Secondary cracks and fissures have also been observed but are beyond the scope of this analysis.

Normal fault slip vectors have the peculiarity of being concordant with the gravity vector. Therefore, with both types of surface brittle deformation occurring in the vicinity of possibly re-activated normal faults, the distinction between

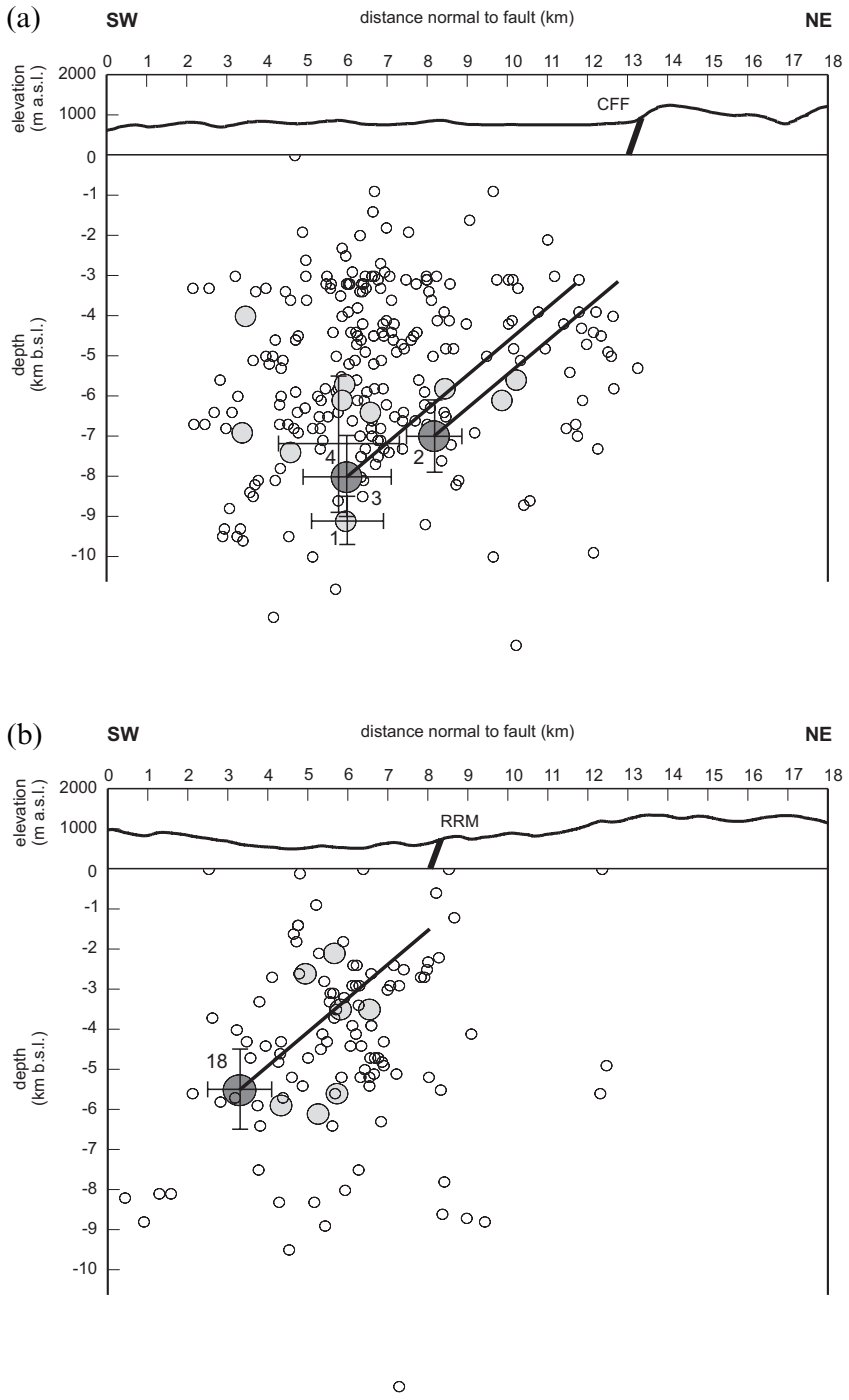

Figure 7. Projections of the fault plane solutions and fault outcrops on SW–NE sections (a) across the CFF (A–A′) and (b) across the CBF-RRM (B–B′). Cross-section traces and selection boxes are shown in Fig. 4.

type A and type B was not straightforward. Qualitative criteria relying on mechanical properties of rocks and soft sediments, geomorphological characteristics of the sites, structural features, and kinematic indicators were thus applied to discriminate one type from the other.

Features induced by ground shaking (type A) formed after the first two main shocks (earthquake numbers 2 and 3) along the CFF, MTF and COF fault scarp and exhibited the following characteristics:

(1) displacement length was a very small proportion of total fault length (3 per cent);

(2) displacements were detected only at the contact between bedrock and slope deposits and soft sediments;

(3) no displacement was ever detected where bedrock was exposed on both walls of the fault;

(4) no displacement was detected where the ground flattens;

(5) slip features followed the contact between bedrock and slope deposits even where the fault scarp had retreated;

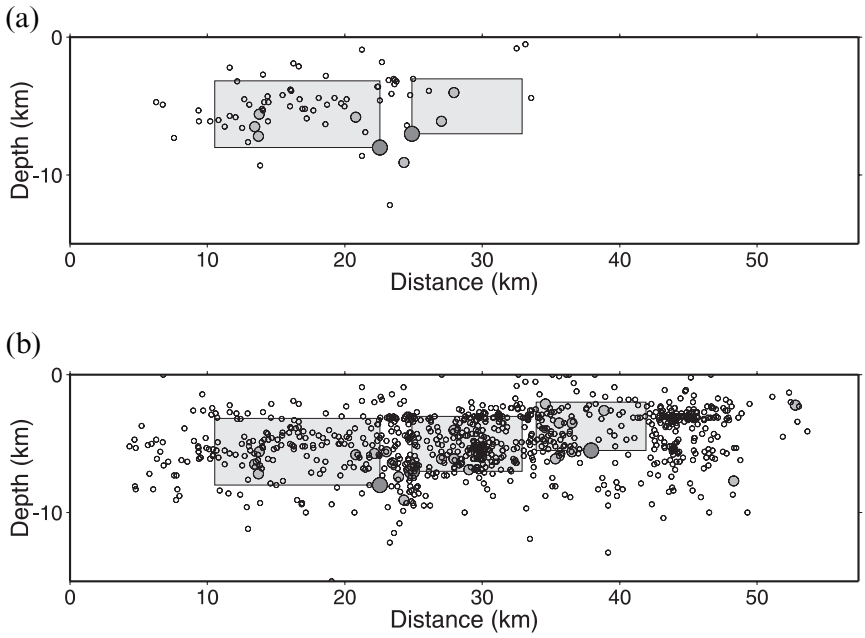

Figure 8. Longitudinal section C–C′: (a) early aftershocks of 1997 September 26, recorded by the SSN temporary network before 1997 October 3; (b) all aftershocks shown in Fig. 4.

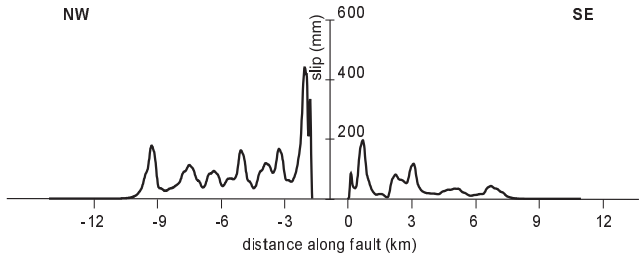

Figure 9. Slip distribution along-fault for the 00:33 (right) and 09:40 (left) events obtained by multiplying the source time functions (at a station in Assisi) by the estimated rupture velocity (Zollo *et al.* 1999) and projecting the derived slip history along the directivity unit vector.

(6) there was always accordance between slip vector and maximum slope direction;

(7) the slip vector was maximum on topographic highs and minimum (tends to zero) in topographic lows;

(8) slip vectors measured across narrow stream incisions had opposite directions.

Features ascribed to type B, however, formed in the southern area after the third main shock (earthquake number 18). Although no faults had been previously mapped in this area, on the Col Beccariccio SW slope a bedrock fault scarp is clearly exposed and is aligned with the coseismic ruptures (see CBF and RRM in Fig. 6). Tectonic features found along the RRM lineament exhibited the following characteristics:

(1) ruptures cut across the surface regardless of the local morphology;

(2) ruptures cut through the rocks regardless of their mechanical properties;

(3) ruptures were mostly continuous;

(4) ruptures exhibited coherent mesoscale structural features;

(5) coseismic slip, inferred by composing vectors of maximum vertical and horizontal displacements, pitched at about 60° to the SE, in good agreement with the CBF slickenside lineations.

A summary of the observed offsets versus fault strike is plotted in Fig. 10.

DISCUSSION

The CFFS belongs to a complex geodynamic framework that includes an active west-plunging subduction driving an east-orientated orogenic progression with a consequent crustal extension in the rear that dominates the tectonic style of the region. In this framework, major earthquakes may occur where the easternmost normal faults of the Apennines record Pleistocene–Holocene tectonic activity. Numerical modelling of the stress pattern in this region shows that insights into fault behaviour and their correlation with local seismicity are needed to produce reliable models of long-term (interseismic) tectonic stress accumulation (Negredo *et al.* 1999). Such analysis would help to predict location, geometry and mechanism of major earthquake faulting.

The 1997–1998 Colfiorito seismic swarm is an intriguing example in this perspective. In fact, the complex geological structure of the CFFS (Fig. 2) includes several individual small-size faults that are difficult to correlate with the seismogenic sources. Unfortunately, surface geological effects that occurred on the various branches of the CFFS and in the surrounding areas were very different in nature and mechanism, and their analysis resulted in dissimilar interpretations and deductions (see, for example, Basili *et al.* 1998; Cello *et al.* 1998; Cinti *et al.* 1999).

Considering the positions of the main shock hypocentres (Figs 6 and 7) and source-fault properties (Table 2), it seems very likely that earthquakes 1, 2, 3, and probably 4, originated

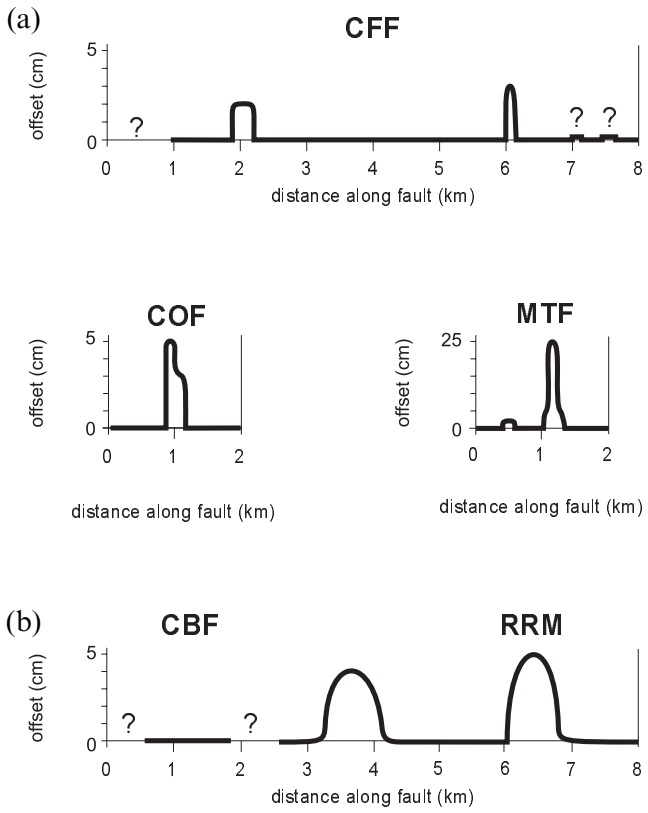

Figure 10. Distribution along-strike (NW–SE) of (a) the offset between bedrock and slope deposits for the CFF, COF, MTF, and CBF fault branches, and of (b) the displacement between bedrock walls for the RRM ruptures.

on the same structure and produced blind normal faulting with ruptures stopping ~4 km below the ground surface (Figs 7 and 8). Given the errors of 1.1 km on hypocentral depth (event 3 in Table 1), the uncertainty of ~2 km in fault width, and the indeterminacy of the fault plane dip of $\pm 14^\circ$ associated with focal mechanisms (Helffrich 1997), the top edge of the fault has to be deeper than 500 m below the ground surface. Earthquake number 18, however, originated on a different structure, and the fault plane solution for this earthquake requires normal faulting with coseismic rupture stopping at about 2 km below the ground surface. Taking into account errors as above, it is possible that fault number 18 intersects the ground surface.

These arguments support the following interpretation of geological effects. Earthquakes 1–4 did not break the surface, and the offsets between bedrock and slope deposits observed along the correlative fault scarps should be interpreted as an effect of ground-shaking. This suggests a slip-rate strengthening behaviour of the CFF gouge (Marone & Scholz 1988), supported also by the strong decrease of seismicity at the upper transition from high- to low-velocity layers (~1.5–3 km). Considering the errors associated with the solution of earthquake number 18, however, the surface ruptures observed along the RRM alignment could be interpreted either as surface faulting or as brittle accommodation of an extensional forced fold.

The kinematic properties of earthquakes 1–4 and 18 provide an estimation of subsurface fault length, down-dip width and directivity (Table 2 and Fig. 6). As observed in large-size earthquakes, early aftershocks define the dimension of the main shock fault planes, and late aftershocks define the total ruptured volume of rock (e.g. Dietz & Ellsworth 1990; Richins *et al.* 1987). Likewise, in this case of moderate-size earthquakes, the main shock fault planes mostly overlap the distribution of early aftershocks (Fig. 8a), independently confirming the estimated subsurface dimension of the fault.

The aftershock distribution across-strike plunges southwestwards (cross-sections, Fig. 7) in accordance with the predicted fault dip, and is bordered by the projections to depth of the surveyed fault planes (Fig. 4). The aftershock depth distribution along-strike (longitudinal section, Fig. 8) becomes thinner from NW to SE, in accordance with the depth distribution of the main shocks, and shows that much of the accompanying deformation in the southeastern area is located near the ground surface. We observe also that the dimension along-strike of the deformed volume of rock is far greater than the total subsurface length of the main shock fault planes and, in turn, of the faults exposed at the ground surface.

The above observations are consistent with the reactivation at depth of relatively steep (~40°) fault planes related to the clearly steep outcropping planes of the CFFS. These are the nearest geological structures to the east of the source-fault top edges among the easternmost principal normal faults in the region.

The average strain field derived from slickenside lineation analysis (Fig. 3) seems to be strictly correlated with the strain field deduced from the earthquake focal mechanisms of the three main events (Table 2), suggesting a possible correlation between the growth of the CFFS over geological time (since Early Middle Pleistocene) and its coseismic behaviour.

The slip distribution along the combined fault related to events 2 and 3 (Fig. 9) has a maximum in the central sector of the total ruptured area which corresponds to the best exposed portion of the CFF and also to the lowermost portion of the hanging-wall topographic relief (Fig. 6). As such, the slip distribution observed during earthquakes 2 and 3, which represents most of the total slip of the swarm, could be related to the long-term cumulative subsidence of the Colfiorito Basin. The similarity between the coseismic slip and the long-term cumulative displacement probably indicates a seismogenic source producing earthquakes like the ones that occurred in 1997. In any case, if faults 1–4 were to interact, fracturing as a single structure, a maximum magnitude of $M_S = 6.4$ (Utsu & Seki 1954) and a slip distribution similar to 1997 ruptures would be expected.

CONCLUSIONS

We analysed and combined the results of geological and seismological observations of the 1997 Umbria-Marche earthquake swarm. We explored the relationships between the structural features detected by geological field surveys and the main shock fault planes ($M > 5.5$) modelled by seismological recordings. The low-magnitude seismicity played an essential role in the interpretation by constraining the dimension and location of the deformed volume of rock.

Although earthquakes 1–3 seem to have reactivated a previously mapped active normal fault (CFF), no surface faulting was detected along its trace. In the case of earthquake number 18, tectonic ruptures (RRM) due to either surface warping or

possibly surface faulting occurred in an area where pre-existing normal faults were neither mapped nor clearly visible in the field.

The total length of the normal faults exposed in the area is about two-thirds of the subsurface maximum fault length predicted by the instrumental data. However, the best exposures of the fault in the field and their associated geological structures are in agreement with the slip distribution derived from the source kinematics.

The test case of the Colfiorito Fault System offered a unique opportunity to study the mechanisms related to the retreat and bending of a west-plunging subduction. The good agreement between the reduced stress tensor derived from fault plane kinematic indicators and the observed main shock focal mechanisms suggests a long-term persistence and coaxiality condition of the regional strain field. This fact allows us to consider a single earthquake-generating mechanism as being active probably since the Early Middle Pleistocene, and supports the use of data analysed in this work in constraining tectonic models. Therefore, we expect that the analysis of long-term structures that could be associated with low-magnitude seismicity will improve, at least in well-known fault systems, our understanding of long-term tectonic stress loading.

ACKNOWLEDGMENTS

Seismometric data were supplied by ING and SSN, while the geological field survey was supported by IRTR-CNR (GNDT project). C. Doglioni, S. Ward, G. Valensise, C. Bosi and R. Sabadini are acknowledged for useful discussions. A. Zollo is thanked for giving us his results before publication. Comments made by George Helffrich and an anonymous reviewer improved the manuscript.

REFERENCES

Amato, A. *et al*., 1998. The 1997 Umbria-Marche, Italy, earthquake sequence: a first look at the main shocks and aftershocks, *Geophys. Res. Lett.,* **25,** 2861–2864.

Angelier, J., 1984. Tectonic analysis of fault slip data sets, *J. geophys. Res.,* **89** (B7), 5835–5848.

Angelier, J., 1990. Inversion of field data in fault tectonics to obtain the regional stress—III. A new rapid direct inversion method by analytical means, *Geophys. J. Int.,* **103,** 363–376.

Barba, S., Di Giovambattista, R. & Smriglio, G., 1995. Accessing the Istituto Nazionale di Geofisica Seismic Network Databank (ISDN), *EOS, Trans. Am. geophys. Un.,* **76,** 89.

Barchi, M., Minelli, G. & Pialli, G., 1997. The Crop 03 profile: a synthesis of results on deep structures of the Northern Apennines, *Mem. Soc. Geol. It*., **52,** 383–400.

Basili, R. & Meghraoui, M., 1999. Coseismic and postseismic displacements related with the 1997 Umbria-Marche (Italy) earthquake sequence, *Geophys. Res. Abs.,* **1,** 95.

Basili, R., Bosi, V., Galadini, F., Galli, P., Meghraoui, M., Messina, P., Moro, M. & Sposato, A., 1998. The Colfiorito earthquake sequence of September–October 1997: Surface breaks and seismotectonic implications for the central Apennines (Italy), *J. earthq. Eng.,* **2,** 291–302.

Berardi, R. *et al*., 1998. Strong ground motion during the 1997 Umbria-Marche earthquake sequence (Abstract), *Ann. Geophys.,* **16** (Suppl. 1) C161.

Boncio, P., Ponziani, F., Brozzetti, F., Barchi, M., Lavecchia, G. & Pialli, G., 1997. Seismicity and extensional tectonics in the northern Umbria-marche Apennines, *Mem. Soc. geol. It.,* **52,** 539–555.

Bonilla, M.G., 1988. Minimum earthquake magnitude associated with coseismic surface faulting, *Bull. Assoc. Eng. Geol.,* **25,** 17–29.

Bonilla, M.G., Mark, R.K. & Lienkaemper, J.J., 1984. Statistical relations among earthquake magnitude, surface rupture length, and surface fault displacement, *Bull. seism. Soc. Am.,* **74,** 2379–2411.

Boschi, E., Guidoboni, E., Ferrari, G., Valensise, L. & Gasperini, P., 1997. *Catalogo dei Forti Terremoti in Italia Dal 461 a.C. al 1990,* Istituto Nazionale di Geofisica, Rome (in Italian).

Bosi, C., Coltorti, M. & Dramis, F., 1983. *Carta del Quaternario della conca di Gualdo Tadino,* Unpublished map, CNR-CSGT and Min. Pubbl. Istr., Progetto Morfoneotettonica, Rome.

Calamita, F. & Pizzi, A., 1992. Tettonica quaternaria nella dorsale appenninica umbro-marchigiana e bacini intrappenninici associati, *Studi Geol. Cam.,* **92/1,** 17–25.

Camassi, R., Galli, P., Molin, D., Monachesi, G. & Morelli, G., 1997. Rilievo macrosismico preliminare del terremoto umbro-marchigiano di settembre-ottobre 1997, *Ingegneria Sismica,* **6/97,** 50–54.

Cattaneo, M., De Luca, G., Gorini, A., Michelini, A., Monachesi, G., Ponziani, F. & XGUMS (eXperimental Group for Umbria-Marche Seismicity), 1998a. Umbria-Marche earthquake sequence: the contribution of the Umbria, Marche and Abruzzo local seismic networks, *Ann. Geophys.,* **16** (Suppl. 1), C162.

Cattaneo, M., Michelini, A., Milana, G. & XGUMS, (eXperimental Group for Umbria-Marche Seismicity), 1998b. Umbria-Marche earthquake sequence: the GNDT-UNIGE/OGS-DINMA and SSN seismic network, *Ann. Geophys.,* **16** (Suppl. 1), C162.

Cello, G., Mazzoli, S., Tondi, E. & Turco, E., 1997. Active tectonics in the central Apennines and possible implications for seismic hazard analysis in peninsular Italy, *Tectonophysics,* **272,** 43–68.

Cello, G., Deiana, G., Mangano, P., Mazzoli, S., Tondi, E., Ferreli, L., Maschio, L., Michetti, A.M., Serva, L. & Vittori, E., 1998. Evidence for surface faulting during the September 26, 1997, Colfiorito (Central Italy) earthquakes, *J. earthq. Eng.,* **2,** 303–324.

Cinti, F., Cucci, L., Marra, F. & Montone, P., 1999. The 1997 Umbria-Marche (Italy) earthquake sequence: Relationship between ground deformation and seismogenic structure, *Geophys. Res. Lett.,* **26,** 895–898.

Coltorti, M. & Dramis, F., 1988. The significance of slope-waste deposit in the Quaternary of Umbria-Marche Apennines, Central Italy, *Zeit. Geomorph., N.F. Suppl.,* **71,** 59–70.

De Martini, P.M., Marchioni, A. & Valensise, G., 1999. Modelling of elevation changes induced by the 1997–98 Umbria-Marche earthquakes: further evidence for shallow-angle normal faulting, *Geophys Res. Abs.,* **1,** 95.

Deschamps, A., Iannaccone, G. & Scarpa, R., 1984. The umbrian earthquake (Italy) of 19 September 1979, *Ann. Geophys.,* **2,** 29–36.

Di Giovambattista, R. & Barba, S., 1997. An estimate of hypocenter location accuracy in large network: possible implications for tectonic studies in the Italian case, *Geophys. J. Int.,* **129,** 124–132.

Dietz, L.D. & Ellsworth, W.L., 1990. The October 17, 1989, Loma Prieta, California, earthquake and its aftershocks: geometry of the sequence from high-resolution locations, *Geophys. Res. Lett.,* **17,** 1417–1420.

Doglioni, C., 1997. Italy (Sections: Regional geology; Tectonics), in *Encyclopedia of European and Asian Regional Geology,* pp. 414–435, eds Moores, E.M. & Fairbridge, R.W., Chapman & Hall, London.

Doglioni, C., Mongelli, F. & Pialli, G., 1997. Boudinage of the Alpine belt in the Apenninic back-arc, *Mem. Soc. geol. It.,* **52,** 457–468.

Dziewonski, A.M. & Woodhouse, J.H., 1983. Studies of the seismic source using normal-mode theory, in *Earthquakes: Observation, Theory, and Interpretation: Notes from the International School of Physics 'Enrico Fermi' (1982: Varenna, Italy),* pp. 45–137, eds Kanamori, H. & Boschi, E., North-Holland, Amsterdam.

Ekström, G., Morelli, A., Boschi, E. & Dziewonski, A.M., 1998. Moment tensor analysis of the Umbria-Marche earthquake sequence of September-October 1997, *Geophys. Res. Lett.,* **25,** 1971–1974.

Ficcarelli, G. *et al.,* 1997. Cesi, an early Middle Pleistocene site in the Colfiorito Basin (Umbro-Marchean Apennine), central Italy, *J. Quat. Sci.,* **12,** 507–518.

Filippi, L. & Alessandrini, B., 2000. Upper-crustal structure of Central Apennine (Italy) from local earthquakes, *Tectonophysics,* submitted.

Haessler, H., Gaulon, R., Rivera, L., Console, R., Frogneux, M., Gasparini, C., Martel, C., Patau, G., Siciliano, M. & Cisternas, A., 1988. The Perugia (Italy) earthquake of 29 April 1984: a micro-earthquake survey, *Bull. seism. Soc. Am.,* **78,** 1948–1964.

Hancock, P.L., 1985. Brittle microtectonics: principles and practice, *J. struct. Geol.,* **7,** 437–457.

Helffrich, G., 1997. How good are routinely determined focal mechanisms? Empirical statistics based on a comparison of Harvard, ESGS and ERI moment tensors, *Geophys. J. Int.,* **131,** 741–750.

Hunstad, I., Anzidei, M., Baldi, P., Galvani, A. & Pesci, A., 1998. Gps observations of co-seismic displacement of the Umbria-Marche seismic sequence, *Ann. Geophys.,* **16** (Suppl. 1), C163.

Lienert, B.R., Berg, E. & Frazer, L.N., 1988. HYPOCENTER: an earthquake location method using centered, scaled, and adaptively least squares, *Bull. seism. Soc. Am.,* **76,** 771–783.

Marone, C. & Scholz, C.H., 1988. The depth of seismic faulting and the upper transition from stable to unstable slip regimes, *Geophys. Res. Lett.,* **15,** 621–624.

Meghraoui, M., Bosi, V. & Camelbeeck, T., 1999. Fault fragment control in the 1997 Umbria-Marche, central Italy, earthquake sequence, *Geophys. Res. Lett.,* **26,** 1069–1072.

Menichetti, M., 1992. Evoluzione tettonico-sedimentaria della valle di Gubbio, *Studi Geologici Camerti,* **92/1,** 155–163.

Negredo, A.M., Carminati, E., Barba, S. & Sabadini, R., 1999. Numerical modelling of the stress accumulation and seismotectonics in central Italy, *Geophys. Res. Lett.,* **26,** 1945–1948.

Olivieri, M. & Ekström, G., 1999. Rupture depths and source processes of the 1997–98 earthquake sequence in central Italy, *Bull. seism. Soc. Am.,* **89,** 305–310.

Pialli, G., Barchi, M. & Menichetti, M., 1991. Studi preliminari all'acquisizione dati del profilo CROP 03 Punta Ala-Gabicce, *Studi Geologici Camerti,* Spec. Vol. 1.

Pino, N.A., Mazza, S. & Boschi, E., 1999. Rupture directivity of the major shocks in the 1997 Umbria-Marche (Central Italy) sequence from regional broadband waveforms, *Geoph. Res. Lett.,* **26,** 2101–2104.

Ponziani, F., De Franco, R., Minelli, G., Biella, G., Federico, C. & Pialli, G., 1990. Crustal shortening and duplication of the Moho in the Northern Apennines: a view from seismic refraction data, *Tectonophysics,* **252,** 391–418.

Richins, W.D., Pechmann, J.C., Smith, R.B., Langer, C.J., Goter, S.K., Zollweg, J.E. & King, J.J., 1987. The 1983 Bora Peak, Idaho, earthquake and its aftershocks, *Bull. seism. Soc. Am.,* **77,** 694–723.

Salvini, F., 1998. *The Structural Data Integrated System Analyzer,* Version 2.151b, 27/10/98, Dip. Scienze Geologiche, University of Roma TRE, Rome.

Stramondo, S. *et al.*, 1999. The September 26, 1997 Central Italy earthquakes: coseismic surface displacement detected by SAR interferometry and GPS, and faulting modeling, *Geophys. Res. Lett.,* **26,** 883–886.

Utsu, T. & Seki, A., 1954. A relation between the area of aftershock region and the energy of main shock, *J. seism. Soc. Jpn,* **7,** 233–240.

Wells, D.L. & Coppersmith, K.J., 1994. New empirical relationships among magnitude, rupture length, rupture width, rupture area, and surface displacement, *Bull. seism. Soc. Am.,* **84,** 974–1002.

Zollo, A., Bongiovanni, G., Herrero, A., Marcucci, S. & Milana, G., 1998. The 1997 Colfiorito earthquake sequence (Central Italy): insights on mainshock ruptures from near source strong motion records (Abstract), *Ann. Geophys.,* **16** (Suppl. 1), C164.

Zollo, A., Marcucci, S., Milana, G. & Capuano, P., 1999. The 1997 Umbria-Marche (Central Italy) earthquake sequence: insights on the mainshock ruptures from near source strong motion records, *Geophys. Res. Lett.,* **26,** 3165–3168.